Environmental Progress
& Sustainable Energy

Dependency of the combustion behavior of energy grass and three other types of biomass upon lignocellulosic composition

Journal:	*Environmental Progress*
Manuscript ID	EP-16-381.R1
Wiley - Manuscript type:	Original Manuscript
Date Submitted by the Author:	n/a
Complete List of Authors:	Ma, Ying Guan, Yan Jun Zhang, Kai; Center of Chem. Eng. for Clean Energy, North China Electric Power University Xu, Gang Yang, Yong Ping Stevenson, Paul
Keywords:	Biomass, Kinetics, Combustion, Cellulose
Alternate Keywords:	

Dependency of the combustion behavior of energy grass and three other types of biomass upon lignocellulosic composition

Ying Ma[1], Yanjun Guan[1], Kai Zhang[1*], Gang Xu[1], Yongping Yang[1], Paul Stevenson[2]

1. Beijing Key Laboratory of Emission Surveillance and Control for Thermal Power Generation, North China Electric Power University, Beijing 102206, China

2. School of Engineering, University of Hull, Kingston-upon-Hull, East Riding of Yorkshire, HU6 7RX, United Kingdom

ABSTRACT

The combustion characteristics of four kinds of biomass fuels (energy grass, sawdust, corn cob and walnut shell) are investigated in this paper. All the samples are heated from room temperature to 800 ℃ at multiple heating rates of 10, 20 and 30 °C/min. The effect of hemicellulose, cellulose and lignin components on the pyrolysis and combustion processes of energy grass is explored by comparison to those of the other three types of biomass. The hemicellulose and cellulose content of samples could improve the devolatilization performance during biomass combustion. Furthermore, the comprehensive combustion index suggested herein indicates that the combustion performance of energy grass or walnut shell is limited by their high ash content or their low ratio of cellulose to lignin. Kinetic parameters are obtained by combining the iso-convertional method (OFW and KAS models) and the method of master-plots. The apparent activation energy of the devolatilization stage is higher than that of the char oxidization stage, which is mainly influenced by the lignocellulosic composition.

* Corresponding author: Professor Kai Zhang. Tel: +86 10 61772413. *Email address*: kzhang@ncepu.edu.cn

***Key words*:** Energy grass, Combustion characteristics, Kinetics, Lignocellulosic compositions

1. Introduction

Biomass is an only renewable carbon source, gaining particular attention in energy generation for its neutral CO_2 conversion, low NO_X and SO_2 emissions, and high content of volatiles [1]. Generally, biomass can be converted into heat or liquid fuel by three thermal conversion processes which are pyrolysis, gasification and combustion [2]. Direct combustion is one of the most extensively employed technologies for commercial or industrial utilization of biomass, and is responsible for about 95-97% of the world's bioenergy produced [3-5]. Thermal analysis is regarded as a useful and reliable tool to determine the thermal properties and kinetics of biomass during combustion [6, 7]. The kinetic parameters are essential for the design, control and optimization of industrial equipment [8]. Iso-conversional methods, such as Ozawa-Flynn-Wall (OFW) or Kissinger-Akahira-Sunose (KAS), are commonly used in numerous kinetic studies on biomass combustion without prior knowledge of reaction mechanisms [9-11].

Biomass is generally considered as an organic fuel derived from plants, including wood, agricultural wastes, herbaceous crops and short-rotation energy crops [3, 12]. Up to now, most studies have focused on the combustion of agricultural or woody biomass using thermogravimetric analysis (TGA)，such as wood [13, 14], pine sawdust [15], capsicum stalks [16], straw [17], sunflower [18], corn cob and stover

[19], grape marc (i.e. skin, seed and stalk) [20]. In comparison to other traditional biomass fuels, energy crops are a promising alternative that are cost-effective, and do not generally require particularly fertile soil good soil or high levels of fertilizer and pesticide application [21-24]. Energy grass (A. donax) is a kind of energy crop artificially cultivated and has following advantages: high calorific value (22.76 MJ/Kg), high production (over fifteen years after planting as a perennial plant), and lower land requirement (growing rapidly in sandy, saline-alkali or industrial waste land) [25]. Because of the economical and environmental advantages of the combustion of energy grass, it is pertinent to investigate its thermal properties. However, previous studies on energy grass have been limited and have tended to focus upon the combustion characteristics.

The chemical composition plays crucial role in the thermal conversion of biomass. Cellulose, a polysaccharide with the generic formula $C_6H_{10}O_5$, is the major component of biomass cell walls, hemicellulose is another cell walls component represented by the generic formula $C_5H_8O_4$, and lignin is the aromatic compound built from three highly crosslinked units [26-29]. So far, few investigations focused on the combustion characteristics related to the biomass components. Gani and Naurse [30] found the cellulose and lignin content were important to evaluate the pyrolysis characteristics. Cheng et al. [31] and Kai et al. [32] used artificial biomass components (microcrystalline cellulose, xylan and lignin) to explore the contribution of lignocellulosic components to the thermal process. They found that hemicellulose

combusted easily and the weight loss of lignin covered a broad temperature range.

The aim of current work is to investigate the combustion characteristics of energy grass in comparison to those of sawdust, corn cob and walnut shell. The combustion characteristics are explored as a function of the hemicellulose, cellulose and lignin contents. The kinetic parameters of the four types of biomass are calculated by methods of iso-conversion master-plots.

2. Experiments and method

2.1 Sample preparation

The samples used in this study are energy grass (EG), sawdust (SD), corn cob (CC) and walnut shell (WS). EG, i.e. *A. donax*, is selected from Changping district in Beijing, and SD, CC and WS are from Heilongjiang Province in China. The four kinds of biomass are ground and sieved to pass an aperture of 200 μm in order to reduce the resistance to mass and heat transfer. All the samples are dried in an oven set at 105 °C for 2.0 hours. Their proximate and ultimate analyses are conducted based on the ASTM methods. Furthermore, the contents of hemicellulose, cellulose, and lignin are determined by employing the method stipulated by the National Renewable Energy Laboratory (NREL) [33]. The lignocellulosic compositions are measured three times and the average values are obtained in this study.

2.2 Experiments

The characteristics of pyrolysis and combustion are evaluated using

thermalgravimetric analysis. Each sample of mass 6±0.2 mg is weighed and placed into an alumina crucible. The pyrolysis process is conducted under nitrogen. To remove the air and ensure an inert environment, the samples are flushed by flowing nitrogen, and then heated from room temperature to 800 °C at a heating rate of 20 °C/min with a flow rate of 80 ml/min. The combustion process is instead carried out in oxidative atmosphere (20% oxygen and 80% nitrogen) at multiple heating rates of 10, 20 and 30 °C/min. All the experiments are conducted three times to assure the repeatability.

2.3 Definition of characteristic parameters

In order to clearly describe the pyrolysis and combustion processes, the following parameters are defined by thermogravimetic (TG) curves [21, 34]:

(1) DTG_{max}: the maximum rate of weight loss during thermal decomposition, indicating combustibility of the sample. DTG_{max1} and DTG_{max2} are introduced if there are two peaks in TG profile.

(2) T_P: the temperature which corresponds to the maximum degradation rate, which is an indicator of reactivity. A lower T_P indicates better ignition performance during the combustion process.

(3) T_i: the initial temperature of the thermal conversion process (e.g. the ignition temperature for combustion). As defined by Biagini et al. [34], the initial temperature is determined by the tangential method and is derived from the earliest maximum degradation rate (DTG_{max1}). As shown in Fig. 1, a vertical line

is drawn through point A (DTG_{max1}) intersecting with TG curve at point B. Subsequently an intersection between a tangent through point B and an extended TG initial horizontal line is made at point C, whose corresponding temperature is considered to be the beginning of thermal conversion process.

(4) T_e: the end temperature of thermal degradation (i.e. the burnout temperature for combustion), which is also determined through determination of the tangent, but derived from the latest degradation rate (DTG_{max2}). T_e represents the completion of thermal degradation. Therefore, the vertical line is drawn through point D in Fig.1, and the tangent line through point E is intersected with the extended TG final horizontal line.

(5) D_i: the ignition index [18], which is a measurement of ignition performance of combustion and described as Eq. (1):

$$D_i = \frac{DTG_{max}}{T_p T_i} \quad (1)$$

(6) S_n: the comprehensive combustion index [16], which is used to evaluate general performance of combustion and can be defined as Eq. (2):

$$S_n = \frac{DTG_{max} DTG_{mean}}{T_i^2 T_e} \quad (2)$$

Fig. 1. Definition of characteristic temperature during thermal conversion process

2.4 Kinetic methods

As mentioned above, the Ozawa-Flynn-Wall (OFW) and Kissinger-Akahira-Sunose

(KAS) models are employed to determine activation energy of the combustion of biomass, and the master-plot method is used to determine the reaction mechanism herein.

The degree of conversion of biomass can be written as Eq. (3):

$$\alpha = \frac{m_0 - m_t}{m_0 - m_f} \tag{3}$$

where m_0 and m_f represent the initial and final masses of the sample respectively, while m_t is the mass at any time.

The fundamental rate equation is generally expressed as Eq. (4):

$$\frac{\mathrm{d}\alpha}{\mathrm{d}t} = k(T) f(\alpha) \tag{4}$$

where t is time, T is temperature and $f(\alpha)$ is the reaction function. $k(T)$ denotes the temperature-dependent rate constant, which is defined in terms of the Arrhenius equation:

$$k(T) = A\exp\left(-\frac{E}{RT}\right) \tag{5}$$

where A is the pre-exponential factor, E is the activation energy and R is the universal gas constant. At a constant heating rate β=dT/dt, Eqs. (4) and (5) can be transformed and combined to give the following expression:

$$\frac{\mathrm{d}\alpha}{\mathrm{d}T} = \frac{1}{\beta} A\exp\left(-\frac{E}{RT}\right) f(\alpha) \tag{6}$$

Upon integration of Eq. (6), the following is obtained:

$$G(\alpha) = \int_0^{\alpha} \frac{d(\alpha)}{f(\alpha)} = \frac{A}{\beta}\int_{T_0}^{T} \exp\left(-\frac{E}{RT}\right) dT \tag{7}$$

The OFW model is described by Eq. (8):

$$\ln\beta = \ln\frac{0.0084AE}{\mathrm{R}G(\alpha)} - 1.0516\frac{E}{RT} \tag{8}$$

The KAS model is expressed as Eq. (9):

$$\ln\frac{\beta}{T^2} = \ln\frac{A\mathrm{R}}{G(\alpha)E} - \frac{E}{RT} \tag{9}$$

Based on Eqs. (8) and (9), the apparent activation energy (E) at a given conversion rate can be obtained from linear correlations of $\ln(\beta)$ and $\ln(\beta/T^2)$ versus$1/T$ [9]. The heating rates of 10, 20 and 30 °C/min are selected to calculate the value E herein.

The method of master-plots is regarded as an effective way to determine the reaction mechanism and reaction order n [35, 36]. The integrated function $G(\alpha)$ can be approximated to Eq. (10) since T_0 being zero has little impact on the right-hand side of Eq. (7).

$$G(\alpha) = \frac{A}{\beta}\int_{T_0}^{T}\exp\left(-\frac{E}{RT}\right)\mathrm{d}T \approx \frac{A}{\beta}\int_{0}^{T}\exp\left(-\frac{E}{RT}\right)\mathrm{d}T = \frac{AE}{\beta R}P(u) \tag{10}$$

where $P(u)$ (u=E/RT) is temperature integral. Since $P(u)$ does not have ananalytical solution, the approximate value can be obtained from Doyle [37]:

$$P(u) = 0.00484\cdot\exp(-1.0516u) \tag{11}$$

The generalized master plots method is suitable for different heating schedules [38]. The kinetic triplets (i.e. kinetic models), A and E are constant for a single-step process [39].

Substituting the value α=0.5 into Eq. (10), yields:

$$G(0.5)=\frac{AE}{\beta R}P(u_{0.5}) \tag{12}$$

The following equation is easily derived from Eqs. (10) and (12):

$$\frac{G(\alpha)}{G(0.5)}=\frac{P(u)}{P(u_{0.5})} \tag{13}$$

where $G(\alpha)$ is constant for a given kinetic model, $G(\alpha)/G(0.5)$ denotes the theoretical value, whilst $P(u)/P(u_{0.5})$ is inferred from experimental data. Therefore, the appropriate mechanism function is obtained from Eq. (13). Different expressions of common reaction mechanisms are listed in Table 1 [35].

Table 1 The most common reaction mechanisms for solid state processes [35]

3. Results and discussion

3.1 Biomass characterization

The results of proximate, ultimate and compositional analyses of biomass samples are shown in Table 2. It is essential to give a summary of chemical analysis due to the correlation with thermal performance of biomass [40]. It is obvious that energy grass (EG) has large amount of ash, whilst sawdust (SD), corncob (CC) and walnut (WS) have small content of ash. Lower ash content may be more beneficial to combustion process. Besides, the sequence of volatile content is CC>SD>WS>EG. Table 2 also shows C, H, O, N and S content of biomass, herein the O content is calculated by difference. The content of N and S of EG is a little higher than those of the other three biomass. In addition, there are some differences on lignocellulosic components among biomass samples, SD, CC and WS demonstrate with high content of cellulose,

hemicellulose and lignin respectively.

Table 2 Proximate, ultimate and compositional analyses of biomass samples

3.2 Pyrolysis characteristics

The pyrolysis process is the initial step of biomass combustion. As shown in Fig. 2a, EG (energy grass) undergoes the smallest weight loss, which is in agreement with the results of proximate analysis (Table 2). There are two peaks in the first stage of pyrolysis except for SD (sawdust) in Fig. 2b. One local maxima peak is observed at about 300 °C and the main peak at around 350 °C, which represents the thermal decomposition of hemicellulose and cellulose, respectively. This is consistent with the fact that hemicellulose decompose over the temperature range of 150-350 °C, whilst cellulose break down occurs between 250 and 400 °C [41]. It is worth noting that the first peak of CC (corn cob) is larger than that of WS (walnut shell) or EG mainly due to the higher content of hemicellulose. There is no shoulder peak for SD, indicating that the decomposition of hemicellulose is overlapped by that of cellulose and lignin. The pyrolysis characteristic parameters of the four types of biomass are summarized in Table 3. It is noted that the pyrolysis of EG starts and ends at 278.9 °C and 406.5 °C, respectively, which are lower than those of the three other types of biomass. The maximum weight loss rate of EG or WS is lower while that of SD or CC is higher, indicating the poorer reactivity of EG or WS. This observation is related to their

volatiles content.

Fig. 2. TG and DTG profiles of four biomass under nitrogen atmosphere at a heating rate of 20 °C/min

Table 3 The characteristic parameters of four types of biomass during the pyrolysis process

3.3 Combustion characteristics

Fig. 3 shows the combustion profiles of the four types of biomass as a function of temperature at heating rates of 10, 20 and 30 °C/min. It is evident that the combustion process can be divided into three stages responding to their DTG profiles. The first stage is dehydration from room temperature to approximately 150 °C. The weight losses for different types of biomass are approximately coincidental since all the samples contain a similar amount of moisture. The second stage is devolatilization at temperatures between 150 and 380 °C, which moves to a slightly lower temperature versus pyrolysis in an inert atmosphere. The maximum devolatilization rate of combustion is a little higher than that of pyrolysis. This is because mild heterogeneous oxidation promotes the pyrolytic abstraction of volatile matter [39]. In addition, the main peak appears around 300 °C and the shoulder peak of EG is not distinct during the combustion process, which is probably because the hemicellulose peak has merged with the cellulose peak. This phenomenon can be explained by the alkali ions causing a reduction in the decomposition temperature of cellulose [42]. The last stage is attributed to the oxidation of char in the temperature range of approximately

380~600 °C.

A series of combustion parameters of the four types of biomass, including the ignition index and comprehensive combustion index, are listed in Table 4. It is noted that the ignition temperature of EG is lower than that of WS or SD. This might be attributed to the fact that the higher lignin content in woody plants delayed the ignition [16]. Moreover, in comparison to EG, CC ignites earlier and exhibits the highest reaction rate in the devolatilization stage, since the ignition performance is improved by higher cellulose and hemicellulose content [43]. At a given heating rate, the reactivity (maximum weight loss rate, DTG_{max}) sequence of devolatilization stage is CC>SD>WS>EG, which is consistent with the hemicellulose and cellulose content in fuels. The ignition index (D_i) of EG shows worst ignition performance. Furthermore, the comprehensive combustion index (S_n) is introduced to evaluate the combustion performance. As shown in Fig. 4, S_n increases with elevated heating rate for each biomass. The higher S_n of CC and SD indicates better combustion performance, while S_n of WS and EG is lower. Comparing the difference of chemical composition amongst the four biomasses, the lowest S_n of EG may be attributed to the largest ash content. Both WS and CC exhibits a lower ash content than does EG. However, WS has a poorer combustion performance, which probably results from lower ratio of cellulose to lignin content (0.39) than that of CC (2.1). Therefore, to evaluate the combustion performance of biomass, both ash composition and the ratio of cellulose to lignin content should be taken into consideration.

Fig. 3. TG and DTG profiles of four types of biomass under airat heating rates of 10, 20, 30 °C/min

Fig. 4. Profile of combustion index for the four types of biomass

Fig. 3 presents the effect of heating rate on combustion performance. It can be seen that both the temperature ranges of the devolatilization and char oxidation stages are becoming wider with an increase in heating rate. As the heating rate increases from 10 °C/min to 30 °C/min, the maximum weight loss rates (DTG_{max1}) of EG, SD, CC and WS increase from 6.1 %/min, 13 %/min, 11.5 %/min and 9.5%/min to 18.6 %/min, 34 %/min, 41.6 %/min and 23.2 %/min, respectively. Combining with Table 4, the ignition temperature (T_i) and end temperature (T_e) also move to higher values as the heating rate increases for all the samples, which results from a particle gradient temperature due to limited thermal conductivity. Similar results were also obtained in previous studies [34, 44].

Table 4 Characteristic combustion parameters at heating rates of 10, 20 and 30 °C/min

3.4 Kinetic analysis of combustion

3.4.1 Iso-conversional method

OFW and KAS models are used to analyze the kinetics due to their ability to give a relatively accurate value of activation energy that is independent of the reaction mechanism [9]. Two stages of thermal degradation are investigated assuming single-step reactions for the solid-state process. Taking energy grass (EG) as an

example, Fig. 5 shows that the plot of ln β and ln (β/T^2) versus1/T with respect of conversion rate both give an approximately linear relationship.

The activation energy of EG can be obtained by determining the slope of the fitted lines. The other three types of biomass (SD, CC and WS) are also divided into two stages, and activation energies are acquired using the above method. Almost all the samples present an excellent linear dependency such that correlation coefficients are greater than 0.99. In this study, the average values of E are calculated by OFW and KAS models since they are appropriate to assess the kinetic parameters of thermal process. As listed in Table 5, the average E value of devolatilization stage is higher than that of char oxidation stage. With respect to the lignocellulosic composition of biomass, this might arise from the fact that lignin, whose decomposition rate is lower than cellulose and hemicellulose components, is condensed to char [45]. There is little difference among activation energies (E) of the four types of biomass in devolatilization stage, but for the char oxidation stage, samples of EG and CC show higher E than do SD and WS. This might be attributed to the fact that cellulose with the highest E has an obvious effect on global kinetics and the E value of hemicellulose was higher than that of lignin [46]. SD and WS contain large amounts of lignin, which explains their lower E in the char oxidation stage.

Fig. 5. Plots used to determine the value of E for energy grass for each stage for both OFW and KAS models

Table 5 Activation energy obtained by the OFW and KAS models for two stages for

four types of biomass

3.4.2 The method of master-plots

The average activation energy (E) is calculated by the iso-conversional methods, and then $P(u)$ is obtained using Eq. (11). Fig. 6a shows $P(u)/P(u_{0.5})$ versus α of the devolatilization and char oxidation stages (EG) at different heating rates. It is revealed that the master-plots of $P(u)/P(u_{0.5})$ against α are in very close agreement for the different heating rates. Similar profiles are obtained for the other three samples, indicating that the kinetics of biomass thermal degradation can be approximated as a single-step reaction model. In addition, the theoretical master plots of $G(\alpha)/G(0.5)$ versus α are compared with the experimental curves $P(u)/P(u_{0.5})$ in Fig. 6b. It is found that the EG-oxidation stage matches the theoretical master plot of the first order model F_1, whilst the experimental master plot of EG-devolatilization stage lies between F_2 and F_3 models. Furthermore, the $F_{2.2}$ model is the most appropriate to describe the devolatilization stage of energy grass by plotting more F_n models, as shown in Fig. 6c. Similarly, the kinetic models of the other types of biomass (SD, CC and WS) are determined by comparing the experimental and theoretical mater-plots (Fig. 6d). The pre-exponential factor (A) is estimated by the intercept of the fitted straight lines (Eqs. (8) and (9)) based upon the determined E and $G(\alpha)$. The average A value and corresponding kinetic models are summarized in Table 6. It is evident that A in the devolatilization stage is much higher than that of char oxidation stage for all samples in this study.

Fig. 6. Plots of $P(u)/P(u_{0.5})$ versus α (a) energy grass (b) comparison between theoretical and experimental master-plots of EG at a heating rate of 20 ^{o}C/min (c) determination of the F_n model for energy grass (d) experimental master-plots of $P(u)/P(u_{0.5})$ versus α (SD, CC, WS) and corresponding kinetic models of $G(\alpha)/G(0.5)$ versus α

Table 6 Kinetic parameters and mechanisms for four types of biomass

4. Conclusions

In this work, the combustion characteristics of energy grass are investigated in comparison with sawdust, corn cob, and walnut shell using TGA. The kinetic parameters of combustion are obtained by combining the iso-conversional and mater-plots methods. The main results can be summarized as:

- Compared with the pyrolysis under nitrogen, the devolatilization stage of combustion moves to a slightly lower temperature, and the maximum devolatilization rate is higher under air.
- Lignocellulosic composition plays an important role in the ignition performance. Ignition index increases with increasing hemicellulose and cellulose content of biomass.
- The comprehensive combustion index can be used to describe the combustion performance of biomass. Poor combustion behavior of energy grass is largely due to high ash content, but for walnut shell this can be attributed to the low ratio of cellulose to lignin content.
- The apparent activation energy of the devolatilization stage is higher than that of

the char oxidization stage for the four types of biomass studied. Compared with sawdust and walnut shell, energy grass and corn cob show a higher activation energy.

- The reaction mechanism of devolatilization and char oxidation stages can be expressed by the master-plot method for the four types of biomass.

Acknowledgements

The authors gratefully acknowledge National Natural Science Foundation of China (91434120), National Basic Research Program of China (2015CB251504), Shanxi Province Coal-based Key Scientific and Technological Project (MD2014-03, MD 2015-01), and 111 Project (B12034).

References

[1] Fernandez-Lopez, M., Pedrosa-Castro, G.J., & Valverde, J.L., et al. (2016). Kinetic analysis of manure pyrolysis and combustion processes. Waste Manage., 58, 230-240.

[2] Yurdakul, S. (2016). Determination of co-combustion properties and thermal kinetics of poultry litter/coal blends using thermogravimetry. Renew. Energy, 89, 215-223.

[3] Vassilev, S.V., Baxter, D., & Vassileva, C.G.. (2013). An overview of the behaviour of biomass during combustion: Part I. Phase-mineral transformations of organic and inorganic matter. Fuel, 112, 391-449.

[4] Kocabaş-Ataklı, Z.Ö., Okyay-Öner, F., & Yürüm, Y.. (2014). Combustion characteristics of Turkish hazelnut shell biomass, lignite coal, and their respective blends via thermogravimetric analysis. J. Therm. Anal. Calorim., 119, 1723-1729.

[5] Jones, J.M., Bridgeman, T.G., & Darvell, B., et al. (2012). Combustion properties of torrefied willow compared with bituminous coals. Fuel Process. Technol., 101, 1-9.

[6] Wang, J., & Zhao, H.. (2015). Pyrolysis kinetics of perfusion tubes under non-isothermal and isothermal conditions. Energ. Convers. Manage., 106, 1048-1056.

[7] García, R., Pizarro, C., & Álvarez, A., et al. (2015). Study of biomass combustion wastes. Fuel, 148, 152-159.

[8] Ceylan, S.. (2015). Kinetic analysis on the non-isothermal degradation of plum stone waste by thermogravimetric analysis and integral master-plots method. Waste Manag. Res., 33, 345-352.

[9] Álvarez, A., Pizarro, C., & García, R., et al. (2016). Determination of kinetic parameters for biomass combustion. Bioresour. Technol., 216, 36-43.

[10] Tahmasebi, A., Kassim, M.A., & Yu, J., et al. (2013). Thermogravimetric study of the combustion of Tetraselmis suecica microalgae and its blend with a Victorian brown coal in O_2/N_2 and O_2/CO_2 atmospheres. Bioresour. Technol., 150, 15-27.

[11] Moliner, C., Bosio, B., & Arato, E., et al. (2016). Thermal and thermo-oxidative characterisation of rice straw for its use in energy valorisation processes. Fuel, 180, 71-79.

[12] Demirbas, A.. (2004). Combustion characteristics of different biomass fuels. Prog. Energ. Combust., 30, 219-230.

[13] Lopez-Gonzalez, D., Fernandez-Lopez, M. & Valverde, J.L., et al. (2013), Thermogravimetric-mass spectrometric analysis on combustion of lignocellulosic biomass. Bioresour. Technol., 143, 562-574.

[14] Senneca, O.. (2012). Kinetics of pyrolysis, combustion and gasfication of three biomass fuels. Study of main combustion characteristics for biomass fuels used in boilers. Fuel Process. Technol., 103, 16-26.

[15] Zhao, J.L., Niu, S.L., & Li, Y.J., et al. (2015). Thermogravimetric Analysis and Kinetics of Combustion of Raw and Torrefied Pine Sawdust. J. Chem. Eng. Jpn., 48, 320-325.

[16] Wang, X., Si, J., & Tan, H., et al. (2012). Kinetics investigation on the combustion of waste capsicum stalks in Western China using thermogravimetric analysis. J. Therm. Anal. Calorim., 109, 403-412.

[17] Greenhalf, C.E., Nowakowski, D.J., & Bridgwater, A.V., et al. (2012). Thermochemical characterisation of straws and high yielding perennial grasses. Ind. Crop. Prod., 36, 449-459.

[18] López, R., Fernández, C. & X. Gómez, et al. (2013). Thermogravimetric analysis of

lignocellulosic and microalgae biomasses and their blends during combustion. J. Therm. Anal. Calorim., 114, 295-305.

[19] Sittisun, P., Tippayawong, N., & Wattanasiriwech, D.. (2015). Thermal degradation characteristics and kinetics of oxy combustion of corn residues. Adv. Mater. Sci. Eng., 2015, 1-8.

[20] Valente, M., Brillard, A., & Schönnenbeck, C., et al. (2015). Investigation of grape marc combustion using thermogravimetric analysis. Kinetic modeling using an extended independent parallel reaction (EIPR). Fuel Process. Technol., 131, 297-303.

[21] Qin, K., & Thunman, H.. (2015). Diversity of chemical composition and combustion reactivity of various biomass fuels. Fuel, 147, 161-169.

[22] Ertem, F. C., Neubauer, P., & Junne, S. (2017) Environmental life cycle assessment of biogas production from marine macroalgal feedstock for the substitution of energy crops. J. Clean. Prod., 140, 977-985.

[23] Collazzo, G.C., Broetto, C.C., & Perondi, D., et al. (2017) A detailed non-isothermal kinetic study of elephant grass pyrolysis from different models. Appl. Therm. Eng., 110, 1200–1211.

[24] Scordia, D., Van den Berg, D., & Van Sleen, P., et al. (2016) Are herbaceous perennial grasses suitable feedstock for thermochemical conversion pathways? Ind. Crop. Prod., 91, 350-357.

[25] Guan, Y.J., Ma, Y., & Zhang, K, et al. (2015). Co-pyrolysis behaviors of energy grass and lignite. Energ. Convers. Manage., 93,132-140.

[26] Dorez, G., Ferry, L., & Sonnier, R., et al. (2014). Effect of cellulose, hemicellulose and lignin contents on pyrolysis and combustion of natural fibers. J. Anal. Appl. Pyrpol., 107, 323-331.

[27] Balogun A.O., McDonald A.G. (2016). Decomposition kinetic study, spectroscopic and pyrolytic analyses of Isoberlinia doka and Pinus ponderosa. Bio. Convers. Bioref., 6, 315-324

[28] Lopez-Velaquez, M.A., Santes, V., & Balmaseda, J., et al. (2013). Pyrolysis of orange waste: A thermo-kinetic study J. Anal. Appl. Pyrol., 99, 170-177.

[29] Gai, C., Dong, Y., & Zhang, T. (2013). The kinetic analysis of the pyrolysis of agricultural residue under non-isothermal conditions, Bioresour. Technol., 127, 298-305.

[30] Gani, A., & Naruse, I.. (2007). Effect of cellulose and lignin content on pyrolysis and combustion characteristics for several types of biomass. Am. J. Physiol-Reg. I., 32, 649-661.

[31] Cheng, K., Winter, W.T., & Stipanovic, A.J.. (2012). A modulated-TGA approach to the kinetics of lignocellulosic biomass pyrolysis/combustion. Polym. Degrad. Stabil., 97, 1606-1615.

[32] Kai, X., Yang, T., & Huang, Y., et al. (2011). The Effect of biomass components on the co-combustion characteristics of biomass with coal. 2011 Second International Conference on Digital Manufacturing & Automation; 1274-1278.

[33] Sluiter, A., Hames, B., & Ruiz, R., et al. Determination of structural carbohydrates and lignin in biomass. laboratory analytical procedure (LAP) 2008b;National Renewable Energy Laboratory (NREL).

[34] Biagini, E., Fantei, A., & L. Tognotti. (2008). Effect of the heating rate on the devolatilization of biomass residues. Thermochim. Acta, 472, 55-63.

[35] Chen, C., Ma, X., & He, Y.. (2012). Co-pyrolysis characteristics of microalgae Chlorella vulgaris and coal through TGA. Bioresour. Technol., 117, 264-273.

[36] Zou, S.P., Wu, Y.L., & Yang, M. D.. (2010). Pyrolysis characteristics and kinetics of the marine microalgae Dunaliella tertiolecta using thermogravimetric analyzer. Bioresour. Technol., 101,

359-365.

[37] Doyle, C.D.. (1962). Kinetic analysis of thermogravimetric data. J. Appl. Polym. Sci., 6, 120.

[38] Pérez-Maqueda, L.A., Criado, J.M., & Gotor, F.J., et al. (2002). Advantages of combined kinetic analysis of experimental data obtained under any heating profile. J. Phys. Chem. A, 106, 2862-2868.

[39] Senneca, O., Chirone, R., & Salatino, P.. (2002). A Thermogravimetric study of nonfossil solid fuels. 2. Oxidative pyrolysis and char combustion. Energ Fuels, 16, 661-668.

[40] Balogun, A.O., Lasode, O.A., McDonald, A.G., (2014). Thermo-analytical and physico-chemical characterization of woody and non-woody biomass from an agro-ecological zone in Nigeria. BioResources, 9, 5099-5113.

[41] Chandrasekaran, S.R., & Hopke, P.K.. (2012). Kinetics of switch grass pellet thermal decomposition under inert and oxidizing atmospheres. Bioresour. Technol., 125, 52-58.

[42] Sebestyén, Z., Lezsovits, F., & Jakab, E. et al. (2011). Correlation between heating values and thermogravimetric data of sewage sludge, herbaceous crops and wood samples. J. Therm. Anal. Calorim., 110, 1501-1509.

[43] Pang, C.H., Gaddipatti, S., & Tucker, G., et al. (2014). Relationship between thermal behaviour of lignocellulosic components and properties of biomass. Bioresour. Technol., 172, 312-320.

[44] Taş, S., & Yürüm, Y.. (2011). Co-firing of biomass with coals. J. Therm. Anal. Calorim., 107, 293-298.

[45] Milne, T.. (1979). Pyrolysis-The thermal behavior of biomass below 600 C. A survey of biomass gasification. United states; 2: 95-132.

[46] Sanchez-Silva, L., Lopez-Gonzalez, D., & Villasenor, J., et al. (2012). Thermogravimetric-mass spectrometric analysis of lignocellulosic and marine biomass pyrolysis. Bioresour. Technol., 109, 163-172.

List of figures

Fig. 1. Definition of characteristic temperature during thermal conversion process

Fig. 2. TG and DTG profiles of four biomass under nitrogen atmosphere at a heating rate of 20 °C/min

Fig. 3. TG and DTG profiles of four types of biomass under airat heating rates of 10, 20, 30 °C/min

Fig. 4. Profile of combustion index for the four types of biomass

Fig. 5. Plots used to determine the value of E for energy grass for each stage for both OFW and KAS models

Fig. 6. Plots of $P(u)/P(u_{0.5})$ versus α (a) energy grass (b) comparison between theoretical and experimental master-plots of EG at a heating rate of 20 ^{o}C/min (c) determination of the F_n model for energy grass (d) experimental master-plots of $P(u)/P(u_{0.5})$ versus α (SD, CC, WS) and corresponding kinetic models of $G(\alpha)/G(0.5)$ versus α

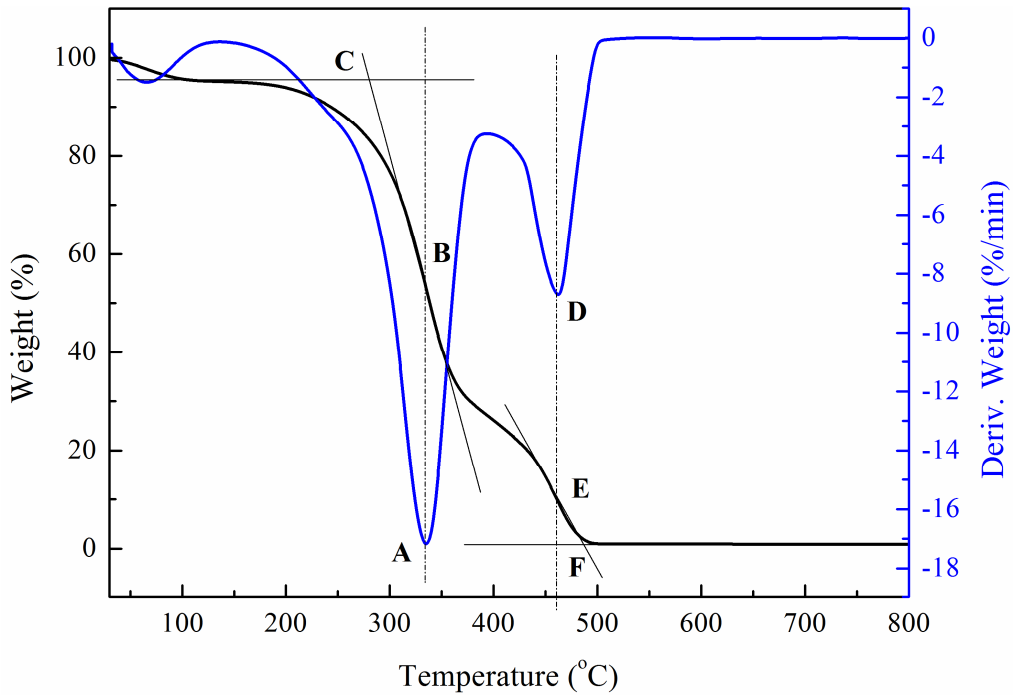

Fig. 1.

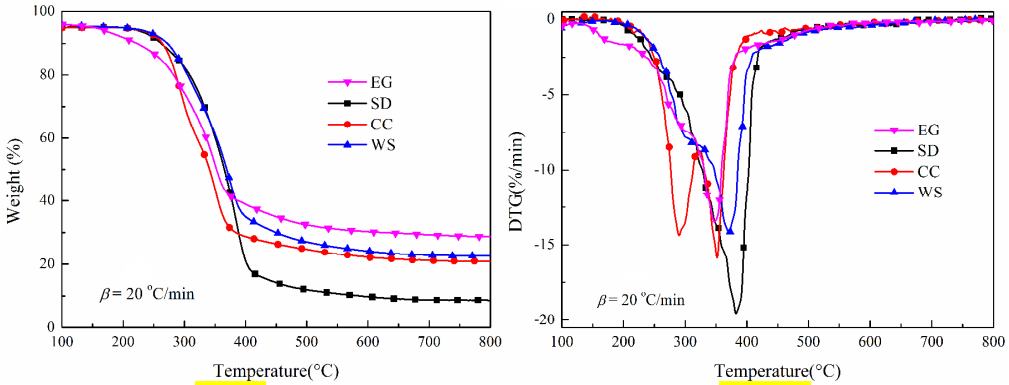

(a) TG (b) DTG

Fig. 2.

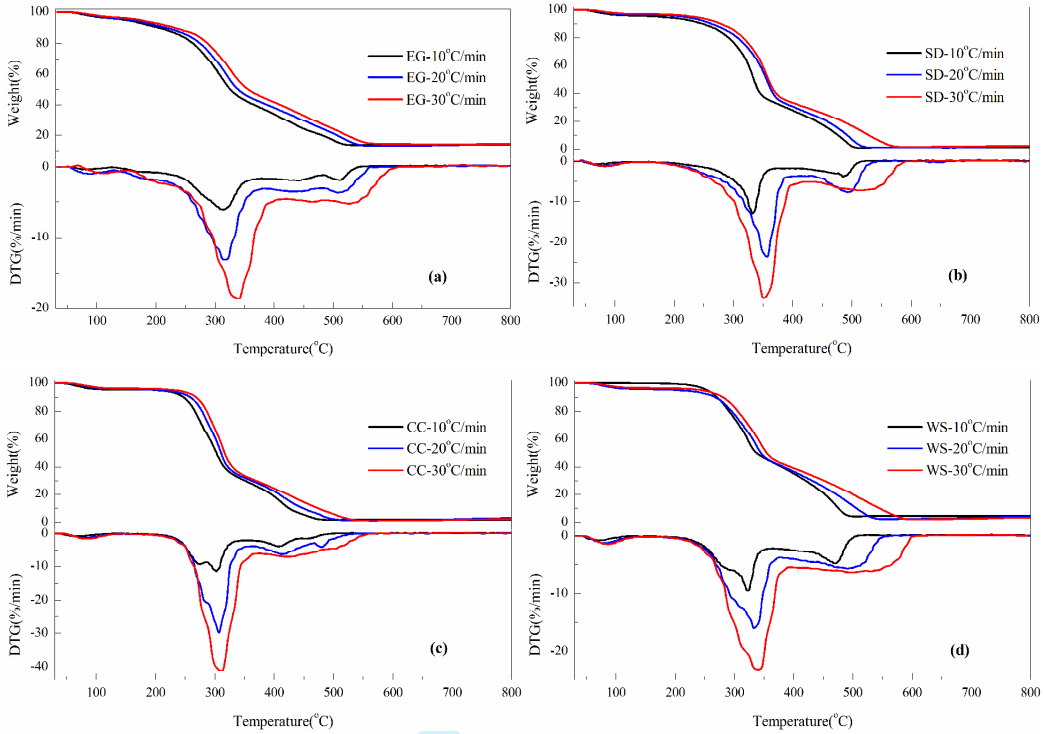

Fig. 3.

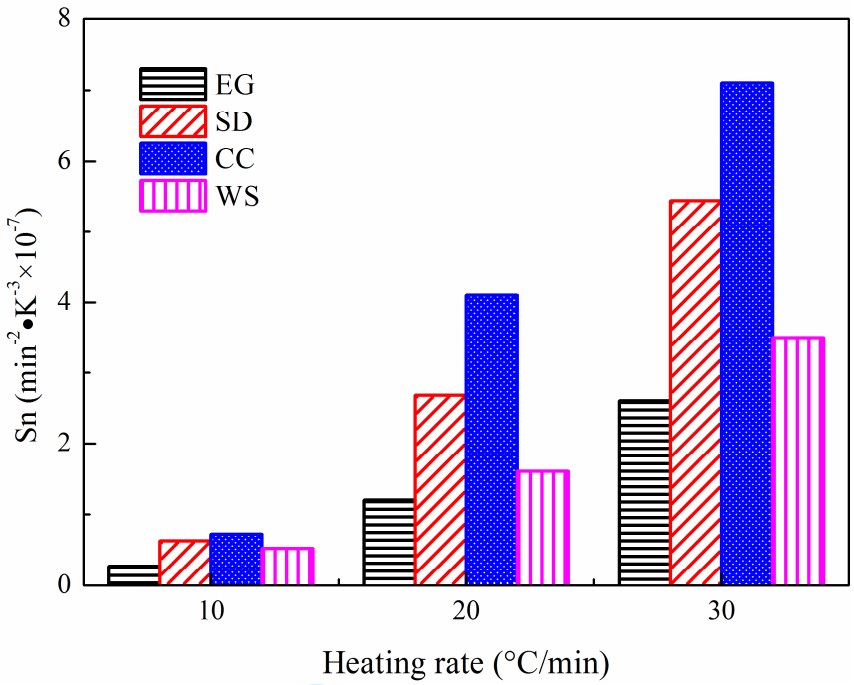

Fig. 4.

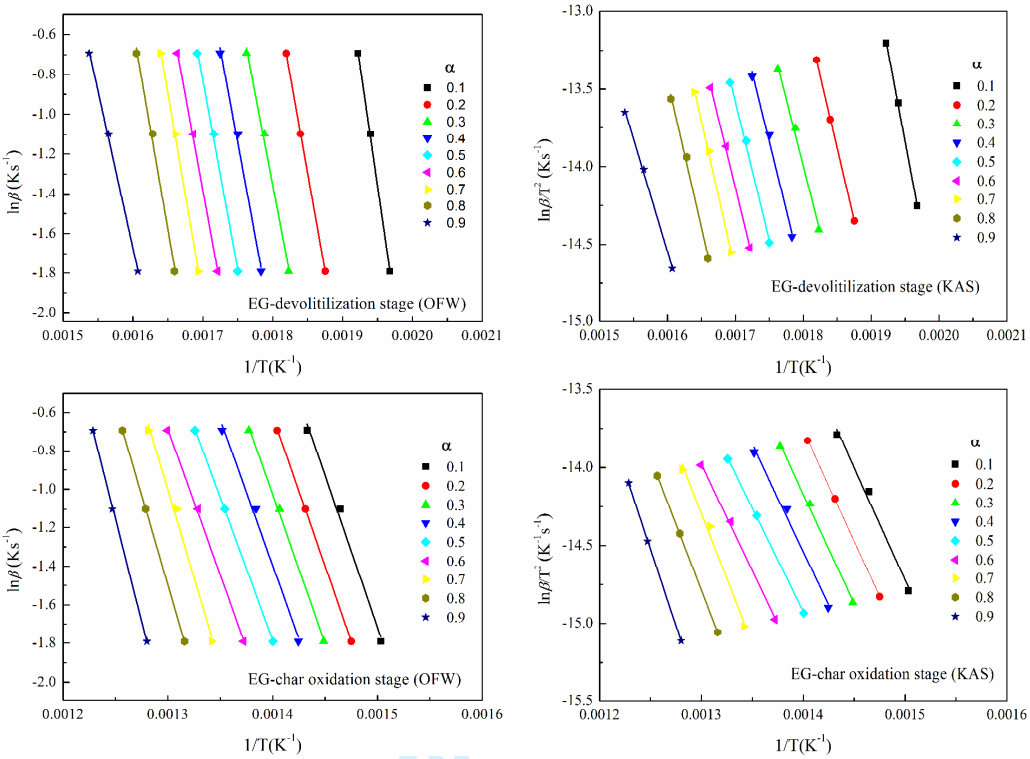

Fig. 5.

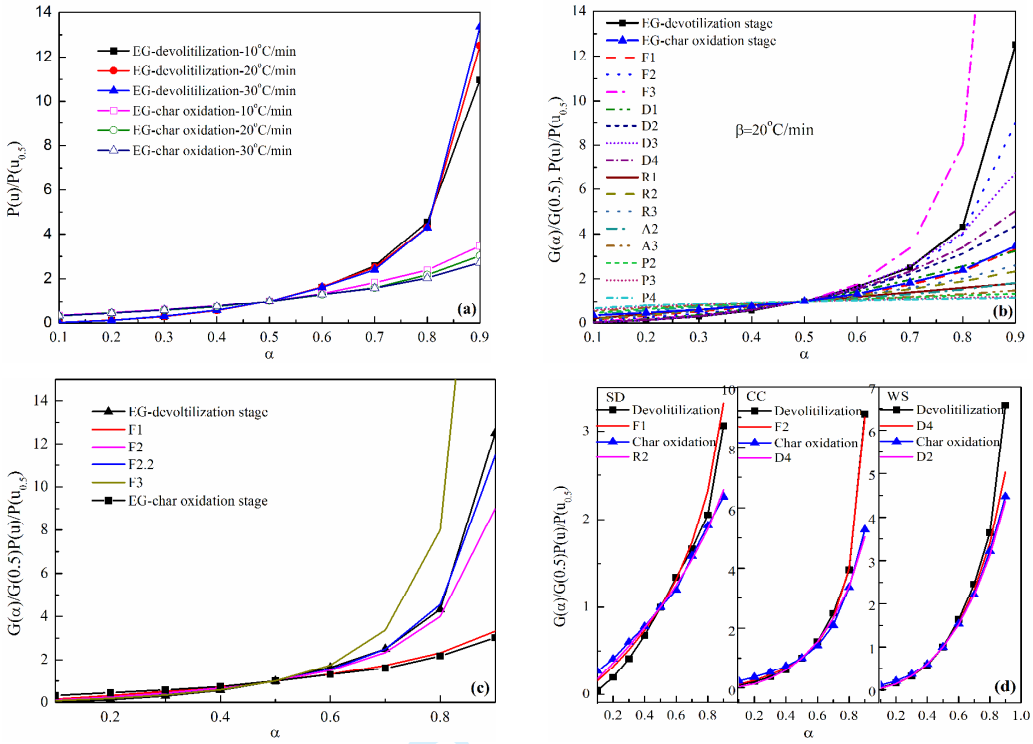

Fig. 6.

List of tables

Table 1 The most common reaction mechanisms for solid state processes [35]

Table 2 Proximate, ultimate and compositional analyses of biomass samples

Table 3 The characteristic parameters of four types of biomass during the pyrolysis process

Table 4 Characteristic combustion parameters at heating rates of 10, 20 and 30 °C/min

Table 5 Activation energy obtained by the OFW and KAS models for two stages for four types of biomass

Table 6 Kinetic parameters and mechanisms for four types of biomass

Table 1

Proximate, ultimate and compositional analyses of biomass samples

	Proximate analysis[a] (wt. %)				Ultimate analysis[b] (wt. %)					Compositional analysis (wt. %)		
	Moisture	Vol	Ash	FC[c]	C	H	O[d]	N	S	Hemicellulose	Cellulose	Ligin
EG	7.25	61.55	16.30	14.90	36.09	5.10	34.27	1.47	0.37	15.04	25.09	23.73
SD	7.65	76.80	0.95	14.60	44.72	6.37	39.86	0.65	0.10	22.53	42.02	34.42
CC	6.90	79.40	1.23	12.47	50.22	6.73	35.30	0.12	0.10	37.43	36.72	17.50
WS	7.20	73.54	1.97	17.29	50.65	6.27	33.92	0.28	0.11	21.62	18.90	48.73

[a]as received basis
[b]air dry basis
[c]The content of FC is calculated by difference
[d]The content of O is calculated by difference

Table 2

The most common reaction mechanisms for solid state processes [34]

Mechanisms	Symbol	$f(\alpha)$	$G(\alpha)$
Order of reaction			
First-order	F_1	$1-\alpha$	$-\ln(1-\alpha)$
Second-order	F_2	$(1-\alpha)^2$	$(1-\alpha)^{-1}-1$
Third-order	F_3	$(1-\alpha)^3$	$[(1-\alpha)^{-2}-1]/2$
Diffusion			
One-way transport	D_1	0.5α	α^2
Two-way transport	D_2	$[-\ln(1-\alpha)]^{-1}$	$\alpha+(1-\alpha)\ln(1-\alpha)$
Three-way transport	D_3	$1.5(1-\alpha)^{2/3}[1-(1-\alpha)^{1/3}]^{-1}$	$[1-(1-\alpha)^{1/3}]^2$
Ginstling-Brounshtein equation	D_4	$1.5\,[(1-\alpha)^{1/3}-1]^{-1}$	$(1-2/3\alpha)-(1-\alpha)^{2/3}$
Limiting surface reaction between both phases			
One dimension	R_1	1	α
Two dimensions	R_2	$2(1-\alpha)^{1/2}$	$1-(1-\alpha)^{1/2}$
Three dimensions	R_3	$3(1-\alpha)^{2/3}$	$1-(1-\alpha)^{1/3}$
Random nucleation and nuclei growth			
Two-dimensional	A_2	$2(1-\alpha)[-\ln(1-\alpha)]^{1/2}$	$[-\ln(1-\alpha)]^{1/2}$
Three-dimensional	A_3	$3(1-\alpha)[-\ln(1-\alpha)]^{2/3}$	$[-\ln(1-\alpha)]^{1/3}$
Exponential nucleation			
Power law, n =1/2	P_2	$2\alpha^{1/2}$	$\alpha^{1/2}$
Power law, n = 1/3	P_3	$3\alpha^{2/3}$	$\alpha^{1/3}$
Power law, n = 1/4	P_4	$4\alpha^{3/4}$	$\alpha^{1/4}$

Table 3

The characteristic parameters of four types of biomass during the pyrolysis process

Samples	T_i (°C)	T_s (°C)	T_p (°C)	T_e (°C)	DTG_{max} (%/min)	Residue (%)
EG	278.9	297.8	347.6	388.5	-13.57	28.77
SD	318.4	-	382.9	411.5	-19.59	8.70
CC	265.2	286.9	351.1	390.0	-16.00	20.92
WS	306.5	300.6	370.8	406.5	-14.31	22.57

Table 4

Characteristic combustion parameters at heating rates of 10, 20 and 30 °C/min

Sample	Heating rate	Devolitilization stage				Char oxidation stage						
		Temperture Range	T_i	T_{p1}	DTG_{max1}	Temperture Range	T_{p2}	T_e	DTG_{max2}	char	D_i	S_n
	(°C/min)	(°C)	(°C)	(°C)	(%/min)	(°C)	(°C)	(°C)	(%/min)	(%)	($\times10^{-7}$)	($\times10^{-7}$)
EG	10	187-378	259.2	313.4	-6.1	378-544	509.7	524.2	-1.9	13.93	0.22	0.27
	20	193-383	270.2	313.5	-13.1	383-577	506.8	541.6	-3.7	14.64	0.47	1.20
	30	191-410	272.9	341.6	-18.6	410-609	527.5	555.3	-4.9	14.40	0.60	2.6
SD	10	156-379	296.0	331.6	-12.0	379-516	486.2	505.0	-3.8	1.47	0.46	0.63
	20	158-390	298.0	357.6	-23.9	390-544	492.5	517.7	-7.8	2.06	0.76	2.68
	30	151-427	310.7	349.3	-34.0	427-591	511.0	564.9	-7.3	2.38	1.10	5.44
CC	10	196-354	254.7	301.9	-12.5	354-498	407.4	473.9	-3.8	1.71	0.47	0.72
	20	188-362	266.3	306.1	-30.4	362-543	411.4	483.5	-6.3	3.13	1.20	4.10
	30	179-375	306.6	310.9	-41.6	375-567	420.1	530.1	-7.0	2.24	1.50	7.10
WS	10	197-357	274.7	321.3	-9.5	357-506	468.2	489.5	-4.8	4.45	0.35	0.52
	20	175-380	282.5	334.5	-15.9	380-551	491.5	532.0	-5.7	3.37	0.54	1.60
	30	170-391	288.2	343.4	-23.2	391-600	499.3	576.5	-6.4	3.21	0.72	3.50

Table 5
Activation energy obtained by the OFW and KAS models for two stages for four types of biomass

Sample	Devolitilization stage			Char oxidation stage		
	OFW	KAS	Average	OFW	KAS	Average
EG	154.0	152.3	153.15	126.5	120.8	123.65
SD	117.5	113.6	115.50	94.1	86.5	90.30
CC	173.0	172.5	172.76	161.2	158.0	159.6
WS	133.9	131.0	132.45	85.4	77.6	81.50

Table 6
Kinetic parameters and mechanisms for four types of biomass

Smaple	*E*(KJ/mol)	Model	*f(α)*	*A*(s^{-1})
EG- devolitilization stage	153.2	F_1	1-α	9.24E+15
EG-char oxidation stage	129.0	$F_{2.2}$	$(1-\alpha)^{2.2}$	2.34E+08
SD- devolitilization stage	115.5	F_1	1-α	7.68E+9
SD- char oxidation stage	90.3	R_2	$2(1-\alpha)^{1/2}$	8.27E+03
CC- devolitilization stage	172.8	F_2	$(1-\alpha)^2$	2.79E+19
CC- char oxidation stage	159.6	D_4	$1.5\,[(1-\alpha)^{1/3}-1]^{-1}$	7.49E+15
WS-devolitilization stage	132.4	D_2	$[-\ln(1-\alpha)]^{-1}$	9.70E+09
WS- char oxidation stage	81.6	D_4	$1.5\,[(1-\alpha)^{1/3}-1]^{-1}$	3.35E+03